ANALYSIS OF LATTICE-GAS CELLULAR AUTOMATON MODELS FOR TUMOR GROWTH BY MEANS OF FRACTAL SCALING*

Sebastiano de Franciscis

Department of Electromagnetism and Physics of Matter
Institute "Carlos I" for Theoretical and Computational Physics
University of Granada, Spain

Haralambos Hatzikirou

Department of Pathology, The University of New Mexico
Albuquerque, New Mexico, USA

Andreas Deutsch

Department of Innovative Methods of the Computing
Center for Information Services and High Performance Computing
Technische Universität Dresden, Germany

(Received April 4, 2011)

Mathematical modeling of tumor development has become a real hype within the last decade. The abundance of mathematical models has created a great need for the validation of their biological relevance. Recently, in order to characterize the tumor growth dynamics, Brú *et al.* have determined some statistical properties of both *in vitro* and *in vivo* solid tumor-surfaces by using fractal scaling analysis. Surprisingly, for all tumor surfaces, the statistical observables converged to a unique set of critical exponents which indicates some common features of tumor growth dynamics (linear growth rate, growth activity limited to the outer rim of the tumor mass and diffusion of newborn tumor cells on the surface from lower to higher curvature regions, typical of Molecular Beam Epitaxy (MBE) Universality). Here, we develop and analyze a lattice-gas cellular automaton (LGCA) model of solid tumor growth. Random walk dynamics are assumed for tumor cell migration and a density-dependent birth process describes the cell mitotic dynamics. Fractal scaling analysis shows that for any parameter variation the model interface dynamic follows Edward–Wilkinson (EW) Universality, which differs from experimental findings. However, the model recovers some features, *i.e.* linear growth rate for tumor size and proliferative activity restricted to the outer layer, observed in experiments.

DOI:10.5506/APhysPolBSupp.4.167
PACS numbers: 05.70.Np, 05.50.+q, 68.35.Ct, 87.10.Hk

* Presented at the 2nd Summer Solstice International Conference on Discrete Models of Complex Systems, Nancy, France, June 16–18, 2010.

1. Introduction

At the beginning of 60s Eden formulate one of the first discrete automata model, in attempting to describe solid tumor growth [1]. Recently, there is a boom of new mathematical models describing various aspects of tumor growth and development. Different mathematical models have been developed in order to describe features of tumor development, like front velocity, necrotic core and proliferative rim dynamics, interactions with the extracellular medium and vasculogenesis, with and without the exposure to chemicals and radiation [2, 3, 4]. A central problem in the mathematical modeling of biological processes is the evaluation of its model biological relevance. In particular, for the problem of tumor development numerous models have been proposed but the methods to check their consistency with experiments or medical observations are sometimes ambiguous or qualitative. Researchers have tried to compare different characteristics of their models such as growth speed, spatio-temporal pattern formation, tumor cell population evolution with *in vivo* or *in vitro* observations. Brú *et al.* [6] have claimed, on the evidence of their experimental investigation of in vivo and in vitro tumor samples, that all avascular solid tumors share the same fractal surface dynamics [5, 6, 7]. In particular, these exponents are typical of the MBE/MH (Molecular Surface Dynamic/Mullins–Herring) surface dynamics [8], characterized by particles/cells generated (or deposited) randomly on the surface and then relaxing towards the highest surface curvature region. This characterization supports the following conclusions on solid tumor growth dynamic: linear growth rate, cell replication activity limited to the outer rim of the tumor mass and displacement of newborn tumor cells on the surface preferably in lower curvature regions. Fractal scaling could be definitively an efficient tool to evaluate tumor models, and to link their mathematical assumptions with real biological properties. In the present study, we analyze a discrete model with diffusive-kinetic dynamics, *i.e.* cells perform random walks and undergo birth/death processes. These are two classical assumptions and a lot of continuous [9, 10, 11] and discrete [12] tumor growth models are based on them. Hatzikirou *et al.* [13, 14] have developed a tumor growth lattice-gas cellular automaton (LGCA) model, which incorporates these diffusion-kinetic assumptions. In this paper, we analyze the growing front in model simulations by using fractal scaling analysis. The main goal is to calculate numerically the statistical observables that allow for the extraction of the critical scaling exponents and to relate them to the proper universality class. We investigate the exponents' dependence on different lattices (square and hexagonal), and on relevant model parameters. Numerical analysis indicates that diffusive dynamics induces the tumor surface developing according to Edward–Wilkinson (EW) Universality, which is not consistent with real *in vitro* and *in vivo* tumors. To

obtain the correct MBE/MH Universality [15] it is necessary to introduce adhesive cell–cell interactions. The paper is organized in the following way: first, we introduce briefly the model, describing its main assumptions and formalizing the mathematical notation. Then we give a basic description of fractal scaling analysis. In the following, we present numerical results about surface critical exponents' extraction, and investigate the compatibility of our model with some appropriate universality class. Finally, some suggestions for future tumor modeling approaches are given.

2. The model

We consider a lattice-gas cellular automaton [16] defined on a two-dimensional regular lattice $\mathcal{L} = L_x \times L_y \in \mathbb{Z}^2$, where L_x, L_y are the lattice dimensions. Let b denote the coordination number of the lattice, that is $b = 4$ for a square lattice and $b = 6$ for a hexagonal lattice, respectively. Cells move on the lattice with discrete velocities, *i.e.* they hop at each time step from a given node to a neighboring one, as determined by the cell velocity. The set of velocities for the square lattice is represented by the two-dimensional channel velocity vectors $\boldsymbol{c_1} = \begin{pmatrix} 1 \\ 0 \end{pmatrix}$, $\boldsymbol{c_2} = \begin{pmatrix} 0 \\ 1 \end{pmatrix}$, $\boldsymbol{c_3} = \begin{pmatrix} -1 \\ 0 \end{pmatrix}$, $\boldsymbol{c_4} = \begin{pmatrix} 0 \\ -1 \end{pmatrix}$, $\boldsymbol{c_5} = \begin{pmatrix} 0 \\ 0 \end{pmatrix}$, while for the hexagonal lattice it is $\boldsymbol{c_1} = \begin{pmatrix} 1/2 \\ \sqrt{3}/2 \end{pmatrix}$, $\boldsymbol{c_2} = \begin{pmatrix} 1 \\ 0 \end{pmatrix}$, $\boldsymbol{c_3} = \begin{pmatrix} 1/2 \\ -\sqrt{3}/2 \end{pmatrix}$, $\boldsymbol{c_4} = \begin{pmatrix} -1/2 \\ -\sqrt{3}/2 \end{pmatrix}$, $\boldsymbol{c_6} = \begin{pmatrix} -1 \\ 0 \end{pmatrix}$, $\boldsymbol{c_7} = \begin{pmatrix} -1/2 \\ \sqrt{3}/2 \end{pmatrix}$, $\boldsymbol{c_8} = \begin{pmatrix} 0 \\ 0 \end{pmatrix}$. In each of these channels, we impose an exclusion principle, *i.e.* we allow at most one cell per channel. We denote by $\tilde{b} = b + b_0$ the total number of channels per node which can be occupied simultaneously, where b_0 is the number of channels with zero velocity (rest channels). We represent the channel occupancy by a Boolean random variable called *occupation number* $\eta_i(\boldsymbol{r}, t) \in \{0, 1\}$, where $i = 1, \ldots, \tilde{b}$, $\boldsymbol{r} = (r_x, r_y) \in \mathbb{Z}^2$ the spatial variable and $t \in \mathbb{N}$ the time variable. The $\tilde{b}$-dimensional vector

$$\boldsymbol{\eta}(\boldsymbol{r}, t) := (\eta_1(\boldsymbol{r}, t), ..., \eta_{\tilde{b}}(\boldsymbol{r}, t)) \in S$$

is called *node configuration* and $S = \{0, 1\}^{\tilde{b}}$ the automaton *state space* (see Fig. 1). We define a *total node density* as the sum of node densities

$$n(\boldsymbol{r}, t) := \sum_{i=1}^{\tilde{b}} \eta_i(\boldsymbol{r}, t)\,.$$

The *global configuration* is given by

$$\boldsymbol{\eta}(t) := (\boldsymbol{\eta}(\boldsymbol{r}, t))_{\boldsymbol{r}\in\mathcal{L}}\,.$$

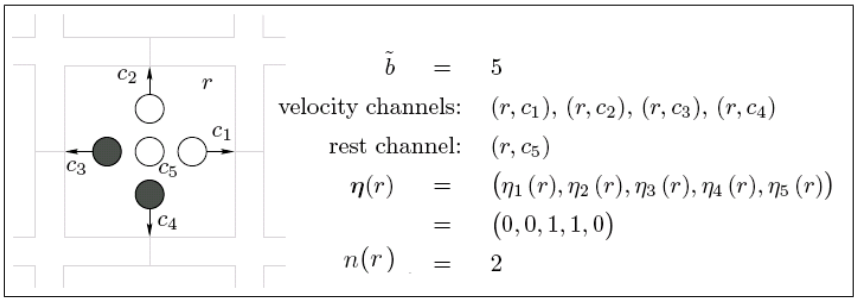

Fig. 1. Example of node configuration in a lattice-gas cellular automaton: channels of node r in a two-dimensional square lattice ($b = 4$) with one rest channel ($b_0 = 1$). Gray dots denote the presence of a cell in the respective channel.

2.1. LGCA dynamics

In our automaton model, cell dynamics are defined by rules. Automaton dynamics arise from the repetition of three rules (operators): propagation (P), reorientation (O) and growth (R). In particular, the combination of reorientation and propagation operators describe [14] cell motion while the growth operator controls the change of the local number of cells on a node. In the following, we describe these operators in detail.

2.1.1. Propagation (P)

The propagation step is deterministic and it is governed by an operator P. By the application of P all cells are transported simultaneously to nodes in the direction of their velocity, *i.e.* a cell residing in channel $(\boldsymbol{r}, \boldsymbol{c}_i)$ at time k is moved to a neighboring channel $(\boldsymbol{r} + m\boldsymbol{c}_i, \boldsymbol{c}_i)$ during one time step. Here, $m \in \mathbb{N}$ determines the speed and $m\boldsymbol{c}_i$ is the translocation of cell. Cells residing on rest channels do not move since they have zero velocity. We note that this operator is mass and momentum conserving.

2.1.2. Reorientation (O)

The reorientation operator is responsible for the redistribution of cells among the velocity channels of a node, providing a new node velocity distribution. Here, we assume that cells perform random walks. A possible

choice for the corresponding transition probabilities is

$$P\left(\boldsymbol{\eta} \to \boldsymbol{\eta}^{O}\right)(\mathbf{r}, t) = \frac{1}{Z}\delta\left(n(\boldsymbol{r}, t), n^{O}(\boldsymbol{r}, t)\right) , \tag{1}$$

where $Z = \sum_{\boldsymbol{\eta}^{O}(\boldsymbol{r},t)} \delta(n(\boldsymbol{r}, k), n^{O}(\boldsymbol{r}, k))$ is a normalization factor. The Kronecker δ guarantees the mass conservation of this operator. Simply, we choose one configuration at random among those with the same number of cells as the initial one (see Fig. 2). The particular choice for the reorientation operator is one out of various possible ways to describe random motion by means of LGCA models [16]. This choice greatly simplifies the possible analytical derivation of the equations describing the meso- and macroscopic evolution of the automaton [13, 14].

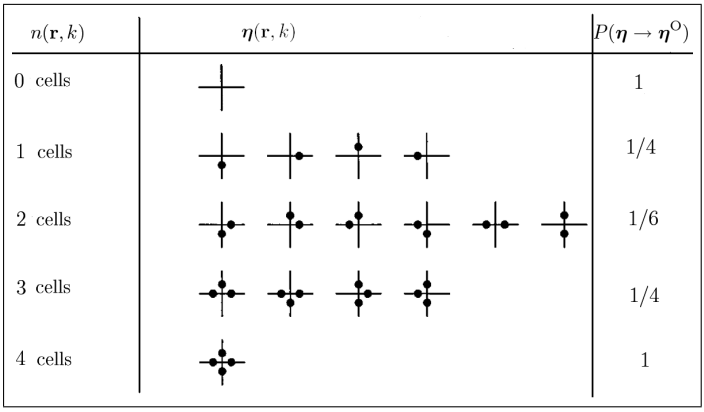

Fig. 2. Reorientation rule of random motion. The first column corresponds to the number of cells on a node $n(\boldsymbol{r}, k)$ at a time k, with capacity $\tilde{b} = 4$. The middle column indicates all the possible cell configurations on node and the transition probability of obtaining a certain configuration is shown in the right column.

2.1.3. Cell kinetics ($\boldsymbol{R}$)

In our model we take into account only mitotic processes (and neglect cell death). We assume that tumor cells can divide only if they have just a few competitors on the node, *i.e.* the cancer node density $n(r, t)$ should be lower than a threshold $\theta_{\mathrm{M}} < \tilde{b}$. The probability of mitosis r_{M} is a function of tumor node density

$$n^{R}(\boldsymbol{r}, t) := \begin{cases} n(\boldsymbol{r}, t) + 1, & \text{w.p.} \quad r_{\mathrm{M}} \quad \text{if} \quad n(\boldsymbol{r}, t) \le \theta_{\mathrm{M}} \\ n(\boldsymbol{r}, t)\,, & \text{else} \end{cases} \tag{2}$$

where w.p. denotes "with probability". In practice, at time t one adds a cell in the node with coordinates $\boldsymbol{r}$ in a randomly chosen free channel, with

probability r_{M}. In a more complete formulation an additional population of "necrotic cells" (dead cells) model is considered [13]. These "interact" with tumor cells when the total node density exceeds θ_{N}, assuming that the nutrient consumption is critical and inducing tumor cell necrosis. Generally, the precise definition of these interactions is a difficult and ambitious task. For *in vivo* tumors the complexity of the interacting phenomena cannot be captured easily by computational models. However, necrotic core tumor interactions are not relevant in analyzing tumor front fluctuation dynamics since necrosis typically occurs some distance away from the tumor front and in our work it has been disregarded.

3. Basics of fractal scaling analysis

Physical systems such as surfaces growing on a substrate by a particle deposition–relaxation process often have a fractal self-affine nature; such systems have been mathematically described both by using continuous Langevin equations and discrete models [17]. The main information that can be extracted from these systems is the spatio-temporal evolution of some statistical observables, such as the dispersion of the surface height around the mean value calculated on the whole surface. These statistical observables typically have a power-law dependence in space and time. The dominant dynamic process may be characterized by measuring the value of the power-laws' exponents, also called scaling critical exponents (for details see [18]). Taking into consideration the fractal scaling analysis of the experimental results found by Brú *et al.* [5,6], here we describe a way to define a surface for the propagating front of a 2D tumor growth LGCA model, and the respective method of scaling exponents measurements, trying to establish relations between the local microscopic rules (birth/death process, re-orientation process) and the surface behavior dynamics (defined by the critical exponents).

A self-affine surface is represented by a height function $h(\vec{x},t)$[1], that is the height coordinate r_y of the surface for the substrate point described by coordinates $\vec{x}$ at time t, having the scaling properties

$$h(\lambda\vec{x},\omega t) = \lambda^{\alpha}\omega^{\beta}h(\vec{x},t)\,, \tag{3}$$

where α, β and $z=\frac{\alpha}{\beta}$ are the scaling exponent; z governs the characteristic surface correlation length dynamic $\xi \propto t^{\frac{1}{z}}$. β is called the *growth exponent*, while α is the *roughness exponent* and z is the so-called *dynamic exponent*.

[1] Alternatively, it is defined as the furthermost occupied node in L_y direction, for each $r_x \in L_x$.

This scaling exponent can be measured by the local surface width $W(l,t)$ and the correlation function $C(l,t)$ defined as

$$W(l,t) = \left\langle \left\langle \sqrt{\langle h^2 \rangle_l - \langle h \rangle_l^2} \right\rangle_L \right\rangle_r ,$$
$$C(l,t) = \sqrt{\left\langle \left\langle \left(h(\vec{x}) - h\left(\vec{x} + \vec{l}\right)\right)^2 \right\rangle_L \right\rangle_r} , \tag{4}$$

where $\langle \cdot \rangle_l$ is the mean value over a window of size l, $\langle \cdot \rangle_L$ over different windows of the system of total size L [2], and $\langle \cdot \rangle_r$ over different replicas r (*i.e.* system realizations), see Fig. 3. These two quantities follow similar

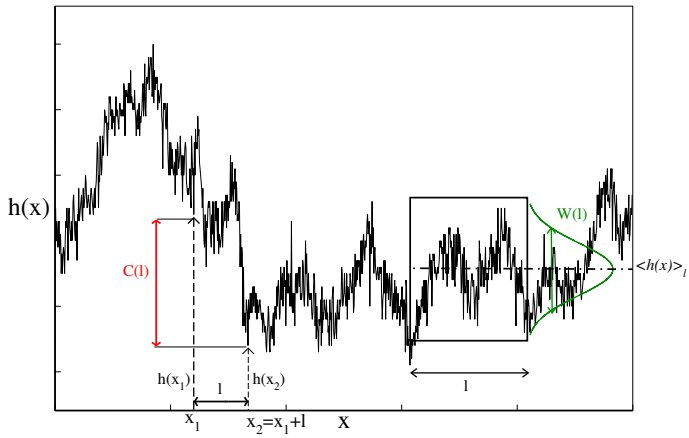

Fig. 3. The correlation function $C^2(l,t) = \langle (h(x_1,t) - h(x_2 = x_1 + l, t))^2 \rangle$ is defined as the mean square height difference among all pairs of surface points $(x, y = h(x,t))$ placed at a distance d from x. The local surface width $W(l,t)$ is the mean of the local variances of $h(x)$, calculated around a mean height $\langle h(x) \rangle_l$ over a domain of fixed size l.

power laws in t and l

$$C(l,t) \approx W(l,t) \propto t^{\beta} f\left(\frac{l}{\xi}\right) , \tag{5}$$

where $f\left(\frac{l}{\xi}\right)$ is the scaling function, dependent only on the value of the correlations size with respect to the system size

$$f(u) = \begin{cases} u^{\alpha_{\text{loc}}} & u \ll 1 \\ \text{const.} & u \gg 1 \end{cases} . \tag{6}$$

[2] More rigorous definitions could be given by $\langle f \rangle_{l,x} = \int_x^{x+l} f(x') \left(\frac{1}{l}\right) dx'$ and $\langle \langle f \rangle_{l,x} \rangle_L = \int_0^L \langle f \rangle_{l,x} \left(\frac{1}{L}\right) dx$.

The exponent α_{loc} is called the *local roughness exponent*. There are two main categories of scaling behavior. If $\alpha < 1$, this exponent describes both the scaling of large and small-length scales, and $\alpha = \alpha_{\text{loc}}$. For this case $C(l,t)$ and $W(l,t)$ increase until a time t_{thr}, when the characteristic correlation length $\xi \gg l$, and they reach a threshold value $W_{\text{thr}} \approx C_{\text{thr}} \propto l$, as one can observe for example in Fig. 5. On the contrary, when $\alpha > 1$ the small-length scales show a trivial scaling with $\alpha_{\text{loc}} = 1$. This generic picture includes most of the scaling behaviors found so far in models and experiments. Tumor growth has been experimentally shown to obey an infrequent superrough dynamics [5,6], characterized by $\alpha_{\text{loc}} = 1$ and $\alpha > 1$. Using the corresponding scaling function of equation 5, one can see that the long time behavior is $C(l,t) \sim l^{\alpha_{\text{loc}}} t^{\beta^\star}$ (instead of the standard behavior $C(l,t) \sim l^{\alpha}$), where $\beta^\star$ is called the *anomalous growth exponent*, $\beta^\star = (\alpha - \alpha_{\text{loc}})/z$. Therefore, anomalous fluctuations at small scales are particularly relevant in this case. A useful observable measuring α is the Power Spectrum of $h(\vec{x},t)$, namely the spatial Fourier Transform

$$S\left(\vec{k},t\right) = \left\langle \hat{h}\left(\vec{k},t\right), \hat{h}\left(-\vec{k},t\right)\right\rangle_r = k^{-(2\alpha+1)} s(k\xi)\,, \tag{7}$$

where the scaling function has the form

$$s(u) = \begin{cases} u^{2\alpha+1} & u \ll 1 \\ \text{const.} & u \gg 1 \end{cases}\,. \tag{8}$$

The most general stochastic Langevin equation describing the dynamic of interface growth function $h(\vec{x},t)$ is

$$\frac{\partial h}{\partial t} = G(\vec{x},h,t) + F(\vec{x},t)\,, \tag{9}$$

where $F(\vec{x},t)$ term is responsible for the addition/deposition, in our case "reproduction", of new cells on the surface and $G(\vec{x},h,t)$ dictates their movements and interactions on it. Typically, $F(\vec{x},t)$ is composed of a constant growth rate f plus a white noise $\zeta(\vec{x},t)$, having its first two moments

$$\begin{aligned} \langle \zeta(\vec{x},t)\rangle &= 0\,, \\ \left\langle \zeta(\vec{x},t)\zeta\left(\vec{x'},t'\right)\right\rangle &= 2A\delta^d\left(\vec{x}-\vec{x'}\right)\delta(t-t')\,, \end{aligned} \tag{10}$$

on the other hand $G(\vec{x},h,t)$ is a function of time t, spatial coordinates $\vec{x}$ and surface profile h and it is generally represented by a differential operator. In some simple cases by means of heuristic scaling arguments, deriving spectral properties or applying renormalization group theory, is possible to derive the

theoretical values of the scaling exponents, that depends in general on the geometrical dimension of the surface d. In Table I the universality classes discussed in our work are defined in terms of their set of critical exponents.

While Edward–Wilkinson (EW) dynamic has a diffusive interaction term, typical of particles random motion. On the other hand, the fourth order term corresponds to the Molecular Beam Epitaxy/Mullins–Herring (MBE/MH) Universality, whose scaling exponents are compatibles with the ones measured by Brú *et al.* [6].

TABLE I

Edward–Wilkinson (EW) and Molecular Beam Epitaxy/Mullins–Herring (MBE/MH) universality classes, defined in terms of their set of critical exponents α, β and z. The value of critical exponents depend on the geometrical dimension d of the surface.

	$G(\vec{x}, h, t)$	α	β	z
EW	$D\nabla^2 h$	$\frac{2-d}{2}$	$\frac{2-d}{4}$	2
MBE/MH	$-K\nabla^4 h$	$\frac{4-d}{2}$	$\frac{4-d}{8}$	4

4. Numerical analysis and results

We have implemented the model described in Sec. 2 on a 2D lattice ($b = 4$ velocity channels) and hexagonal lattice ($b = 6$ velocity channels) lattice $\mathcal{L} = L_x \times L_y$, with $|L_x| = |L_y| = \{1024, 2048\}$[3], lateral periodic boundary conditions and reflecting boundary at L_x (*e.g.* a cell in a velocity channel pointing towards the boundary, is placed — reflected — in the opposite velocity channel). The initial conditions are defined as $n((r_x, 1), 0) = 1$, $\forall r_x \in L_x$. We consider principally the case in which the mitotic threshold is half of the maximum node density, *i.e.* $\theta_{\mathrm{M}} = \tilde{b}/2$, and the number of rest channels $b_0 = 4$.

The height function $h(x, t)$ at x is defined as the y coordinate of the lattice site with the last nonzero cell density at time t, measuring the density of the x-th column starting from $r_y = 1$, see Fig. 4. Alternative definitions of the height function have been considered for lattice gas or percolation front [19,20], producing multivalued surfaces with overhangs. Our definition can be considered as one of the most simplest in order to perform dynamic scaling, and has a good consistency at least in the case of compact tumors observed at short scale, in linear approximation. In the case of more jagged

[3] The notation $|\cdot|$ denotes the cardinality of a given set, *i.e.* $|L_x| = 1024$ when $L_x = [1, 1024]$.

profiles and non linear geometries, more sophisticated definition of the height function have to be considered to obtain a consistent scaling, able to identify the universality class correctly [5].

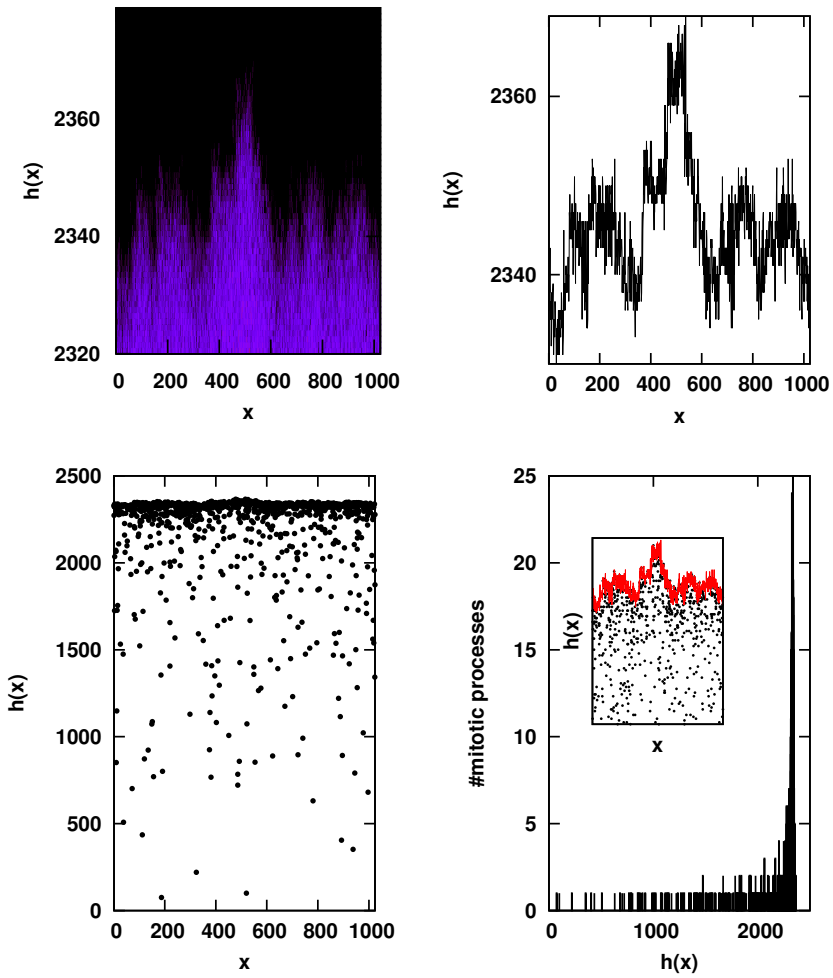

Fig. 4. Top: Front cell density profile (left) and height function $h(x,t)$ (right) for the LGCA model (parameters $\theta_{\mathrm{M}} = 5$, $r_{\mathrm{M}} = 0.1$) on a hexagonal lattice (number of rest channels $b_0 = 4$) with x size $L = 1024$. Bottom: Mitotic events at a given time step (left and right figure) and their frequency distribution *vs.* the height level $y = h(x)$. Mitotic activity is highly concentrated on a thin front layer, consistent with the hypothesis [6] about linear growth concentrated on the outer rim of the tumor mass.

In all cases studied, the front velocity, which is defined as the slope of the mean height $\langle h(t)\rangle_x$, was found to be constant (see [13]). We note that the height function $h(x,t)$ provides the actual position of the front, as in Fig. 4 up-right. The cell proliferation activity is concentrated within a narrow region close to the front (see the two lower graphs of Fig. 4). The location of the proliferation events is in good agreement with the observations of *in vivo* and *in vitro* tumors [6].

The surface height function $h(x,t)$ exhibits non trivial spatio-temporal scaling exponents when varying the mitotic rate r_{M} over a broad range (up to 3 orders of magnitude). The scaling exponent $\beta = \frac{\alpha}{z}$ is evaluated by direct calculation of $W(L,t)$ time slope, while α and z are measured by the data collapse of $W(\cdot,t)$ and $C(\cdot,t)$ time series (see Eq. (5)). The fractal scaling analysis shows that the exponents fit well with EW universality, as it is shown in Figs. 5–7. Variations of the mitotic threshold θ_{M} and of the number of rest channels b_0 does not seem to affect universality, as one can see in Fig. 6. Some differences are observed due to the lattice topology. In particular, on the hexagonal lattice the global width $W(L,t)$, after an initial transient, grows with an exponent typical of the EW regime for a broad range of mitotic rates $r_{\mathrm{M}} \in (0.01, 0.5)$. The stationary regime is observed in our simulations even in the case of small system size, *i.e.* $L_x = 1024$. However, in the square lattice it is more difficult to observe the final growth — stationary — regime, due to a very long transient that follows KPZ dynamics, with $\beta = \frac{1}{3}$, as a result of the square lattice induced symmetry (data not shown), particularly persistent for high r_{M}. The surface correlation functions $C(l,t)$ exhibit also an EW-compatible regime. Moreover, the spatial correlations collapse in a suitable way using both the EW universality spatial α and temporal β exponents, at least for long spatial distances l. The spatial correlations are mainly developing due to the proliferation events, since the random walk dynamics induce only uncorrelated spatial structures. Thus, we can state that the low mitotic probabilities r_{M}, in combination with a short domain size, are responsible for the lack of a sufficiently large number of proliferative events for the building up of significant spatial correlations. From the other hand, with high r_{M} fluctuations in surface roughness reaches saturation rapidly, thus also in this case finite system size play a main role in the observation of the EW regime in the temporal scaling of global width $W(L,t)$. Thus in the limit of low mitotic probability and large system size, the surface front fluctuations increase as a power law with a typical EW exponent for long times.

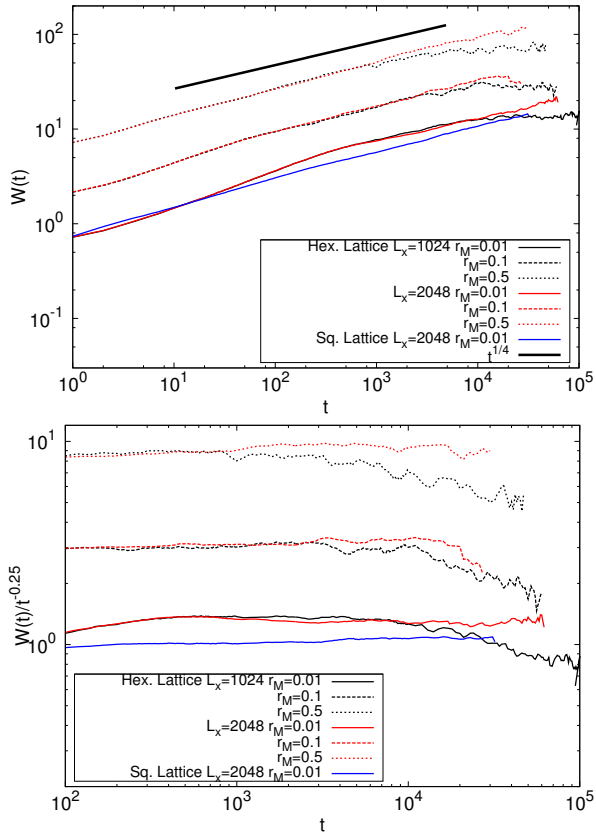

Fig. 5. Global surface width $W(L,t)$ (top) and its scaling with the EW universality β exponent (bottom), for different lattice geometries, system sizes and mitotic rates r_{M}. The mitotic threshold is set to $\theta_{\mathrm{M}} = \tilde{b}/2$. For all cases global width growth is compatible with the typical EW universality scaling Ansatz $W(L,t) \propto t^{\beta}$ with $\beta = \frac{1}{4}$. It is possible, moreover, to observe for size $L = 1024$ the transition between growth regime and threshold regime, as predicted by scaling Ansatz in Eqs. (5) and (6), when the characteristic correlation length reaches the system size. Each curve has been averaged over 50 different realizations (10 realizations for $b_0 = 1$). Curves corresponding to different r_{M} are shifted in y direction for a better visualization.

5. Conclusions and perspectives

In this study, motivated by the work of Brú *et al.* [6], we used fractal scaling analysis to evaluate the suitability of some common assumptions in tumor growth modeling. In particular, we tested the hypothesis that avascular tumor dynamics may emerge from the combination of random cell motion coupled with a stochastic birth process. The corresponding model

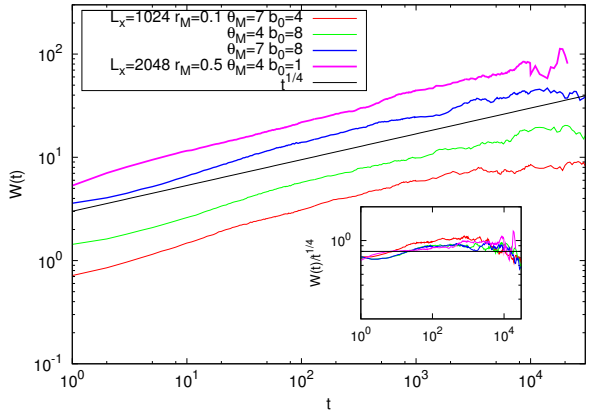

Fig. 6. Global surface width $W(L,t)$ and its scaling with the EW universality β exponent (inset), for systems in a hexagonal lattice, with different mitotic thresholds θ_{M} and mitotic rates r_{M}. Global width growth is compatible with the typical EW universality scaling Ansatz $W(L,t) \propto t^{\beta}$ with $\beta = \frac{1}{4}$. Each curve has been averaged over 10 realizations. Curves are shifted in y direction for a better visualization.

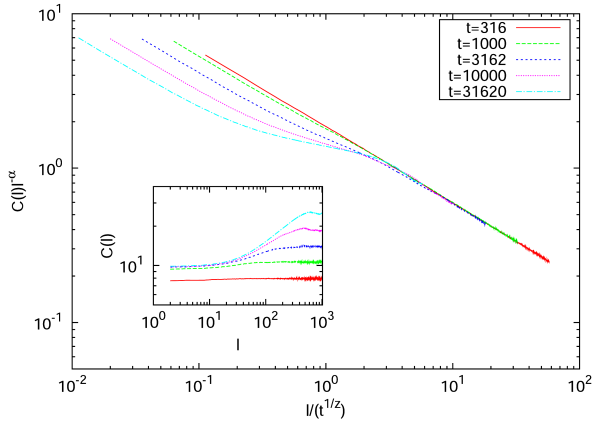

Fig. 7. Collapse of surface correlation functions $C(l,t)$ (Inset: original unscaled functions) calculated at different logarithmic times, for a system on a hexagonal lattice, with $L = 2048$, $b_0 = 4$, using EW universality exponents. Data collapse indicates the compatibility of the surface dynamics with the EW universality scaling Ansatz $C(l,t) \propto l^{\alpha} f(l/t^{1/z})$, described in Sec. 3, at least for $l > 50$. Each curve has been averaged over 30 different realizations.

is motivated by a recently developed LGCA model [13, 14], which can effectively describe the avascular growth phase. The key idea is to check if the resulting spatio-temporal dynamics of the front, described in terms of fractal scaling exponents, match with the ones found by Brú *et al.* [6].

We have considered our model in 2D with appropriate periodic cylindrical boundary conditions, that allow for the development of a well defined 1D front, described by a corresponding height function $h(x,t)$. Then we have measured the self-affine properties of the increasing tumor border in our simulations by means of fractal scaling analysis. Our study provides numerical evidence that our virtual tumor surfaces are compatible with the EW universality, which describes, in the context of surface growth by random particle deposition, a relaxation process that moves the particles towards the local height gradient minimum. It is worth pointing out that the spatially homogeneous migration/proliferation dynamic rules produce non-trivial front structures, usually obtained by one-dimensional models only involving surface particle interactions.

This model is a very simplified view of tumor growth. Actually microenvironment, by means of diffusive signals (nutrients, growth factors *etc.*), ECM components or other stroma interactions, plays a significant role in tumor development. Another point we want to stress out concerns the actual experimental setup limitations of Brú *et al.* [6] in the measure of critical exponents. In fact, critical properties are extracted in *in vivo* samples from 2D cut sections of a 3D tumor mass, while in *in vitro* case the original systems grow just on a plane on the Petri dish. Then one of the main criticisms to their work is related to the finding, in both cases, of 1D MBE universality scaling exponents, measured on a linear front, where a real tumor grows in a three dimensional space, with a 2D spherical surface front. This is still an interesting open question, beyond the scope of this work, so we limited our analysis to 2D planar systems, mimicking better *in vitro* experiments, at least at short scales, where an arc segment can be approximated with a straight line. There are a few studies on self-affine surface growth that consider cut section or geometries different from the Euclidean [7,21]. Then further investigations are required in order to develop scaling techniques for experimental and numerical analysis of tumor front growing in nonlinear geometries (*e.g.* radial growth).

Implementing our model within a hexagonal lattice geometry has some advantages with respect to a square lattice, such as higher order directional isotropy. This effect is expressed in the front dynamics on hexagonal lattices as a shorter temporal dynamic transient, a prominent asymptotic growth dynamics under both size and mitotic rate modulations, and the shorter equilibration of the relevant surface statistical observables. On the contrary, front dynamic on square lattices are characterized by a long r_{M}-dependent KPZ transient.

Our model predicts two of the solid tumor dynamic features claimed by Brú *et al.* [6], *i.e.* proliferation actvity concentrated at the outer rim of the tumor bulk and a linear front velocity. However, the universality class of the

surface front dynamics found here is not the MBE/HM found by Brú *et al.* [6, 5]. Microscopically, the traditional view on MBE dynamics imposes a particle relaxation process which directs particles to the minimum of the surface curvature. The latter suggests us to implement a different reorientation rule, for example dependent on a function of local cell density gradients, in order to find the universality class characterizing real tumors. Please note that MBE dynamics describe a non-local mechanism of motion, in contrast to EW, whereas the curvature "information" is non-local, *i.e.* refers to an extended neighborhood. In a following study, we will introduce a mechanism that provides the desired universality for the surface dynamics. Finally, another very intriguing and important step is the derivation of a coarse-grained partial differential equation for density $\rho(\vec{x}, t)$ in d dimensions, obtained from the microscopic model, by use of standard mean-field techniques [13, 14, 22], and the calculation of the corresponding Langevin equation describing the $(d-1)$-dimensional surface front dynamics for $h(x, t)$.

REFERENCES

[1] M. Eden, Proceedings of the 4th Berkeley Symposium on Mathematics and Probability Vol. 4., ed. by J. Neyman, University of California Press, Berkeley 1961.

[2] L. Preziosi (ed.), *Cancer Modelling and Simulation*, CRC Press, 2003.

[3] *Selected Topics on Cancer Modelling Genesis — Evolution — Immune Competition — Therapy*, Birkhäuser-Springer Ed., 2008.

[4] N. Bellomo, N.K. Li, P.K. Maini, *Math. Model. Meth. Appl. Sci.* **18**, 593 (2008).

[5] A. Brú *et al.*, *Phys. Rev. Lett.* **81**, 4008 (1998).

[6] A. Brú, S. Albertos, J.A. López García-Asenjo, I. Brú, *Biophys. J.* **85**, 2948 (2003).

[7] A. Brú, D. Casero, S. de Franciscis, M.A. Herrero, *Math. Comp. Model.* **47**, 546 (2008).

[8] Z.-W. Lai, S. Das Sarma, *Phys. Rev. Lett.* **66**, 2348 (1991).

[9] A.J. Perumpanani, B.P. Marchant, J. Norbury, *SIAM. J. Appl. Math.* **60**, 463 (2000).

[10] A.J. Perumpanani, J.A. Sherratt, J. Norbury, H.M. Byrne, *Phys.* **D126**, 145 (1999).

[11] J.A. Sherratt, M.A.J. Chaplain, *J. Math. Biol.* **43**, 291 (2001).

[12] M. Marusic, Z. Bajzer, J.P. Freyer, S. Vuk-Pavlovic, *Cell Prolif.* **27**, 73 (1994).

[13] H. Hatzikirou *et al.*, *Comp. Math. Appl.* **59**, 2326 (2010).

[14] H. Hatzikirou, A. Deutsch, *Curr. Top. Dev. Biol.* **81**, 401 (2007).

[15] M. Block, E. Schöll, D. Drasdo, *Phys. Rev. Lett.* **99**, 248101 (2007).

[16] A. Deutsch, S. Dormann, *Cellular Automaton Modeling of Biological Pattern Formation*, Birkhäuser, Boston 2005.

[17] A.L. Barabàsi, H.E. Stanley, *Fractal Concepts in Surface Growth*, Cambridge University Press, Cambridge 2000.

[18] J.J. Ramasco, J.M. Lòpez, M.A. Rodrìguez, *Phys. Rev. Lett.* **84**, 2199 (2000).

[19] A. Brú, D. Casero, *Europhys. Lett.* **64**, 620 (2003).

[20] B. Chopard, M. Droz, M. Kolb, *J. Phys. A: Math. Gen.* **22**, 1609 (1989).

[21] C. Escudero, *Phys. Rev.* **E73**, 020902 (2006).

[22] H. Hatzikirou, S. de Franciscis, F. Peruani, in preparation.